EXPERIMENTS ON THE FLOW AT THE NOSE OF A THIN AIRFOIL

EUGENE RICHARD DOERING

EXPERIMENTS ON THE FLOW AT THE NOSE OF A THIN AIRFOIL

Thesis by

Eugene Richard Doering

Lieutenant, United States Navy

In Partial Fulfillment of the Requirements
For the Degree of
Aeronautical Engineer

California Institute of Technology

Pasadena, California

1959

ACKNOWLEDGEMENTS

Sincere appreciation is extended to Dr. Anatol Roshko, who suggested the idea for this paper and contributed time and guidance towards its completion, and to Ben Williams who helped immensely with the setup of the test apparatus and equipment.

ABSTRACT

An investigation of a family of two-dimensional airfoils was conducted in the Merrill Wind Tunnel at California Institute of Technology, to determine experimentally the effect of camber on an airfoil that stalls at the nose, and to compare the results with a simplified thin airfoil theory, which requires that flow conditions at the nose be similar.

The nine percent thick models had cambers of zero, three, and six percent, and a fourth model with six percent camber had a rear slot at about 70 percent chord.

Tests conducted at Reynolds Numbers of 640,000 and 840,000 showed that the addition of camber to a nose-stalling airfoil tended to make it a trailing-edge staller or partially so, but that by use of the slot, the stall was shifted back to the nose.

Good agreement was obtained in the theoretical and experimental determination of maximum lift for the slotted airfoil, but not for the angle at which this occurred.

TABLE OF CONTENTS

LIST OF FIGURES

LIST OF SYMBOLS

C_{l_o}	=	lift coefficient at zero angle of attack
C_{l_b}	=	basic lift coefficient
$C_{l_{max}}$	=	maximum lift coefficient
$\Delta C_{l_{max}}$	=	difference in maximum lift coefficients
α	=	angle of attack
α_i	=	ideal angle of attack
$\alpha_{i_{ex}}$	=	experimental ideal angle of attack
$dC_l/d\alpha$	=	lift curve slope
dy_c/dx	=	slope of the camber line
x	=	chordwise coordinate
θ	=	angular coordinate of a half circle erected on the chord, corresponding to chordwise coordinate, x.
x_s	=	stagnation point location
ς	=	nose radius of fitting ellipse
δ	=	major axis of ellipse
τ	=	minor axis of ellipse
b	=	thickness parameter
a	=	lift curve slope

INTRODUCTION

Today's fast cruising airplanes are being designed with the thinner type airfoil sections, to reduce drag and thus improve efficiencies. These thinner airfoils have different stalling characteristics than the old thick airfoils.

Basically an airfoil can stall in one of three ways; the trailing edge stall, and two types of leading edge stalls. Reference 1 defines these types as follows:

a) Trailing edge stall - flow separation which commences at the trailing edge and moves forward with increasing angle of attack

b) Leading edge stall - abrupt flow separation near the leading edge without reattachment

c) Thin airfoil stall - flow separation at the leading edge with reattachment at a point which moves rearward with increasing angle of attack.

In addition to the pure type of stalls, leading edge and trailing edge separation can occur in combination, producing a sort of 'hybrid' stall, generally controlled by the leading edge.

Reference 1 presents a survey on symmetrical airfoils and shows that the leading edge type of stalls is peculiar to the thinner airfoils and that the lift curve for such an airfoil is practically linear right up to the stall, instead of being rounded-off, as it is with thick airfoils.

This means that the behavior of a thin airfoil is largely governed by the conditions at the nose of the airfoil. Further, if two airfoils have similar conditions existing at the nose, that is, similar pressure distributions, then the behavior of the two airfoils should be similar.

Inter-related are pressure distribution, stagnation point location, and ideal angle of attack. In thin airfoil theory, ideal angle of attack is that angle of attack for which there is no nose singularity, that is, the stagnation point coincides with the nose of the camber line. Also, it is known that the pressure distribution on a given nose shape is very nearly a function of the stagnation point location, irrespective of camber.

Thus, if two airfoils of different camber but identical nose shapes have similar conditions at the nose, that is, similar pressure distributions and consequently similar stagnation point locations, the two airfoils will differ in angle of attack by an amount equal to the difference of the ideal angles of attack.

Thus, given a symmetrical airfoil, for which the ideal angle of attack is zero, and a similar cambered airfoil, the pressure distribution near the nose of the symmetrical airfoil for angle of attack, α, should exist for the cambered airfoil at α plus the ideal angle of attack, α_i, and likewise the angles of attack for maximum lift should differ by α_i.

Thin airfoil theory provides a method for computing α_i for a given cambered airfoil, and also provides a method for computing the basic lift due to camber, C_{l_b}, which is the lift produced at the ideal angle of attack.

Thus, given the lift curve of a symmetrical airfoil, the lift curve of the cambered airfoil can be determined, simply by shifting the lift curve of the symmetrical airfoil to the right by an amount equal to the ideal angle of attack of the cambered airfoil, and upwards by an amount equal to the basic lift due to camber. Thus, theoretically, $\Delta C_{l_{max}} = C_{l_b}$.

The above hypothesis is discussed in greater detail in Ref. 2 and 3.

Thin airfoil theory does not account for the effects of boundary layer thickening with increase in angle of attack. As the boundary layer thickness increases there is a loss in circulation, which causes the stagnation point to move forward on the under surface of the airfoil. Thus it is expected that there will be some disagreement between actual results and that predicted by thin airfoil theory.

This paper presents the results of an experimental analysis of the effects of adding camber to a thin symmetrical, nose-stalling airfoil, based on the above idea.

The investigation was conducted in the Merrill Wind Tunnel at the California Institute of Technology, Pasadena, California during March and April, 1959.

EQUIPMENT

Four airfoil models were constructed and used in this investigation,

a) Symmetrical

b) 3 percent camber

c) 6 percent camber

d) 6 percent camber, with trailing edge slot.

All models were made of highly polished mahogony, with a brass nose, and waxed. All had 10 inch chords and 20 inch spans.

Airfoil geometry was as follows. Reference 2 makes use of a nose fitting ellipse in its development, thus all four airfoils had elliptic noses. Arbitrarily, the airfoils were chosen to have a nose radius of 0.5 percent and be 9 percent thick. The ellipse, in these coordinates is given by

$$y^2 = 2\varsigma x(1 - x/\delta)$$

where

$$\delta = \tau^2/2\varsigma$$

ς = nose radius

δ = major axis of ellipse

τ = minor axis of ellipse

Accordingly, δ was fixed at 0.81, (normalized).

This ellipse was then joined to the NACA 65-009 airfoil, so that the resulting airfoil had a thickness distribution which was elliptic for the first 40 percent, and 65-009 for the remaining 60 percent, with the maximum thickness of 9 percent at 40 percent

of chord. This then constituted the symmetrical airfoil, and served as the thickness distribution for the cambered airfoils.

The first 10 percent of the airfoil was made of brass, and was used as the nose for all four models, thus maintaining identical nose geometry. It had eight pressure orifices, staggered within the center inch of span, located at the 0.0, 0.1, 0.5, 1.25, 2.5, 5.0, 7.5 (upper), and 7.5 (lower) percent stations (Fig. 1).

The airfoil was cambered using NACA mean lines, numbers 34 and 64, giving 3 percent camber and 6 percent camber respectively, at 40 percent chord. The mid point of the brass nose and the mean line were joined at approximately 10 percent chord, creating a discontinuity in the slope of the mean line at that station; however the airfoil surface was unaffected.

The fourth model was a modification of the 6 percent cambered airfoil. A trailing edge slot was put in at about 70 percent chord, covering 90 percent of span; 1/2 inch at each end and 1 inch in the center being closed.

Fig. 2 shows sketches of the models and the details of the slot geometry; and Table I gives the airfoil coordinates and mean line data.

Circular discs, 15 inches in diameter, were fitted to the sides of the models to approximate two dimensional flow conditions.

Surface pressures were taken from the models by holes which extended from the nose of the model, chordwise, to the rear of the brass nose into spanwise brass tubing, and thence through

the end plates to flexible tubing to a manometer board.

Two mid-chord side mounts and a mid-span sting attached to the under surface of the airfoil supported the models in the wind tunnel test section.

The investigation was conducted in the Merrill Wind Tunnel, which is a single return type with a 32 by 45 inch test section and a 6:1 contraction ratio. Power is supplied by a 75 horse power, constant speed, electric motor, driving a three-bladed electric pitch controlled propeller, which gives a speed range of 0 to 180 mph. Three 32-mesh wire screens were mounted at the entrance to the contracting section to decrease turbulence.

A three component beam balance for measuring aerodynamic forces, a multiple mercury manometer for measuring pressures, and an inclined alcohol micro-manometer for controlling tunnel velocities completed the general test equipment. Fig. 3 shows a model mounted in the tunnel test section.

In addition to the data obtained from the above equipment, several upper surface tuft surveys were made by securing pieces of thread to the model with scotch tape.

A standard pitot tube and an alcohol manometer were used for a special test described in the next section.

EXPERIMENTAL PROCEDURE

For the purposes of this investigation, tunnel corrections were unnecessary, and therefore none were applied to any measured data.

Zero angle of attack was initially set by use of a height gage, aligning the leading edge orifice and the trailing edge with the test section floor. In addition, a pressure balance which checked the initial setting, was obtained for the symmetrical model, from the upper and lower 7.5 percent orifices.

Tunnel velocity was kept constant for each test, during which lift forces and surface pressures were recorded for various angles of attack from minus one degree through maximum lift. Peak pressures and corresponding angles of attack were found by trial and error technique. Severe buffeting limited the amount of data available past the angle of maximum lift.

Each model was tested at two tunnel velocities, corresponding to dynamic pressures of 20 and 40 psf. As tunnel velocity was kept constant, Reynolds Number varied slightly, due to heating but average Reynolds Numbers were 640,000 and 840,000. Each model was retested at 20 psf for reproducibility of results, which was reasonably good.

Finally, upper surface tuft surveys, conducted at 20 psf, were made by observing tufts spaced one inch apart along the chord, at the mid and quarter span stations.

A special test was made on the slotted six percent cambered airfoil, in which the slot was covered with heavy scotch tape on both

surfaces, and the results compared with those of the unslotted six percent cambered model.

The results differed slightly. The slopes of the lift curves and the $C_{l_{max}}$'s of the two models agreed closely, but the angle of attack for $C_{l_{max}}$ was about one-half of a degree greater for the taped model, and the value of C_{l_o} was about eight percent less for the taped model. This means that a slight reduction in camber had been effected in the taped model. However, the results seem close enough that any major differences between the results of the slotted and the unslotted models can be attributed to the slot.

A separate check on the location of the stagnation point was made by measuring the pressures on the three foremost orifices against pitot pressure. Angle of attack was recorded for each orifice when it reached stagnation pressure. The need for this test became apparent only after the symmetrical and three percent cambered airfoils had been dismantled, consequently it was made only on the two six percent cambered configurations.

It was found that the stagnation point location could be determined only to within one-half degree, by this method.

EXPERIMENTAL RESULTS

1. Lift Curves.

Lift data is shown in Fig. 4, for all models at both velocities. First it is seen that $C_{l_{max}}$ for each configuration is independent of velocity, but that the slopes exhibit some Reynolds Number effect, in that they are greater at the higher velocity. The measured values of the lift curve slopes are as follows:

Model	$dC_l/d\alpha$	
	q = 20 psf	q = 40 psf
Symmetrical	4.9	5.3
3 % Camber	5.1	5.5
6 % Camber	5.1	5.5
6 % Camber Slotted	5.1	5.5

These values are consistent with the general effect of Reynolds Number for airfoils of this thickness (Ref. 4).

The symmetrical model has a nearly linear lift curve with only local rounding near $C_{l_{max}}$ for the low velocity test, but a distinct discontinuity for the high velocity test occurring at about the time the pressure peak collapses. According to Ref. 1, this is a characteristic of the thin-airfoil type staller.

The high velocity lift curve also shows less local rounding near $C_{l_{max}}$, tending toward the abrupt leading-edge type of stall. An attempt to investigate this trend was made, but tunnel velocity could not be maintained for high angles of attack for much over dynamic pressure of 40 psf. It was noted, however, that buffeting was much more severe at the stall for the maximum tunnel velocity obtainable.

The lift curve of the three percent cambered airfoil shows signs of rounding off, while that for the six percent cambered model exhibits a very definite rounding off. However, the slotted six percent cambered model shows a lift curve with two linear portions. This change in the slope of the lift curve occurs at about the angle of attack where severe rounding off begins for the unslotted model. Therefore it seems very likely that this change is due to some phenomenon of the slot; it is definitely not due to the suction peak collapse. This occurs at about 15 degrees angle of attack. One other interesting thing is noticed here. It is seen from Fig. 4 that the slotted configuration has a lower value of C_{l_o} and a greater (less negative) angle of attack for zero lift.

2. Tuft Surveys.

Tuft surveys indicated very effectively what was occurring. The results are presented in tabular form as follows:

MODEL:	Symmetrical
TRAILING EDGE:	No separation; turbulence at high angle of attack
LEADING EDGE:	7.5 to 8.0 degrees, separation evident 8.5 degrees, reattachment point between 10 and 20 percent chord
COMMENTS:	Reattachment point progressed rearward with increasing α
MODEL:	3 percent camber
TRAILING EDGE:	8.75 degrees, separation evident 10.0 degrees, separation reached a point between 85 and 90 percent chord 10.5 degrees, separation disappeared
LEADING EDGE:	10.5 degrees, separation evident 11 degrees, reattachment point between 10 and 20 percent chord
COMMENTS:	Reattachment point progressed rearward with increasing α ; no further separation appeared at the trailing edge.
MODEL:	6 percent camber
TRAILING EDGE:	8.5 degrees, separation evident 15 degrees, separation progressed forward of mid chord
LEADING EDGE:	15.5 degrees, separation evident

COMMENTS: Slight recession of trailing edge separation noticed when leading edge separation appeared; however, just prior to stall, trailing edge separation was again forward of mid chord and leading edge reattachment point was between 20 and 30 percent chord.

The results of the six percent cambered model suggested an attempt at boundary layer control, which was done by means of a rear slot located at about 70 percent chord.

MODEL: Slotted 6 percent camber

TRAILING EDGE: No separation

LEADING EDGE: 14.5 degrees, separation evident
15 degrees, reattachment point between 10 and 20 percent chord

COMMENTS: At 17 degrees, which is past the angle of maximum lift, the area forward of the slot was separated, yet the area aft of the slot was not separated and did not even show signs of turbulence.

This last tuft survey certainly shows the effectiveness of the slot. However, the important role of the slot is the fact that it converted the trailing edge stalling six percent cambered model into a thin-airfoil type staller.

With reference to types of stalls, it is noted that although

the three percent cambered configuration showed trailing edge separation, the stall was definitely controlled by separation at the nose. It cannot be definitely stated that the leading edge controlled the stall of the unslotted six percent cambered configuration.

3. Pressure Distribution.

Fig. 5 shows the pressure coefficient versus angle of attack for a representative portion of the recorded data. The pattern presented was similar for each model, varying only in magnitude and in position with respect to the origin of the graph.

The data shown is the pressure variation of the first three orifices (0.0, 0.1, 0.5 percent chord) with angle of attack for the symmetrical model and the slotted six percent cambered model, at a tunnel speed of 40 psf.

The pressure distributions showed the following:

a) of the family of curves of a particular model, the minimum pressure was always recorded at the 0.1 percent orifice, and that the pressure distribution of this orifice formed a sort of envelope about the rest of the family

b) the first four orifices (0.0, 0.1, 0.5, 1.25 percent chord) reached minimum pressures at about the same angle of attack, and succeeding orifices reached minimum pressures

at slightly greater angles of attack, due to collapse of the pressure peak and subsequent redistribution of pressures.

Fig. 6 shows much the same information, but in a slightly different form. Fig. 6 shows the pressure distribution on the nose of the symmetrical airfoil at 20 psf for the four angles of attack at which minimum pressures were recorded at all orifices.

4. Stagnation Point Location.

From Fig. 5 the experimental value of the ideal angle of attack can be determined; that is, the angle of attack at which the leading edge orifice reaches stagnation pressure, as well as the angles of attack at which other orifices reach stagnation value. As was mentioned previously, a special test was made to determine these angles, by recording stagnation pressures at the first three orifices. These values checked well with the values from the pressure distributions, agreeing to within one-half degree, and the results are summarized below:

Model	X_s	α
Symmetrical	0	.5
3 camber	0	1.5

Model	X_s	α
6 camber	0	3.25
	0.001	1.25
	0.005	-1.5
6 camber - slotted	0	4.5
	0.001	2.0
	0.005	0.0

5. Comparison With Theoretical Ideas.

The main concept behind this investigation is that, given the lift curve of a thin symmetrical airfoil and a means of computing ideal angle of attack and basic lift for the corresponding cambered airfoil, the lift curve of the cambered airfoil can be determined.

The hypothesis presumes that thin airfoil behavior is governed by the conditions existing at the nose, and therefore if two airfoils have similar noses, similar conditions should exist at the proper angles of attack. Fig. 7 compares the pressure distribution of the symmetrical airfoil at α of 7.5 degrees with the slotted six percent cambered model at α of 12 degrees, the difference being the measured value of ideal angle of attack for the cambered model ($\alpha_{i_{ex}} = 4.5^{\circ}$).

It is seen that flow conditions for the two airfoils are reasonably similar at the proper angles of attack. From Fig. 4

it is seen that the angles of attack for $C_{l_{max}}$ are 11 and 16 degrees for the symmetrical and slotted six percent cambered model respectively, a difference of 5 degrees, which further supports the hypothesis.

From Ref. 2 and 3, we have the following results. The stagnation point location is given by

$$X_s = \left\{b \tan(\alpha - \alpha_i)\right\}^2$$

where

b = a thickness parameter; 0.98 for this airfoil family

α = angle of attack

α_i = ideal angle of attack

The ideal angle of attack and basic lift coefficient are given by

$$\alpha_i = \frac{1}{\pi} \int_0^{\pi} (dy_c/dx)\, d\theta$$

$$C_{l_b} = 2 \int_0^{\pi} (dy_c/dx) \cos\theta\, d\theta$$

where

dy_c/dx = slope of the camber line

θ = angular coordinate of a half circle erected on the chord corresponding to chordwise coordinate, x.

The latter two equations are based on thin airfoil theory.

Fig. 8 shows the stagnation point location versus angle of attack for theoretical and experimental values. It is seen that,

due to viscous effects, agreement is poor. The following table, which gives theoretical values of X_s, will help to clarify Fig. 8 in the vicinity of the origin.

MODEL	α	X_s (percent chord)
Symmetrical	2.0	0.117 lower surface
	1.0	0.029 " "
	0.0	0.0
	-1.0	0.029 upper surface
	-2.0	0.117 " "
3% camber	2.0	0.084 lower surface
(α_i = 0.322)	1.0	0.013 " "
	0.322	0.0
	0.0	0.003 upper surface
	-1.0	0.051 " "
	-2.0	0.158 " "
6% camber	2.0	0.054 lower surface
(α_i = 0.643)	1.0	0.004 " "
	0.643	0.0
	0.0	0.012 upper surface
	-1.0	0.079 " "
	-2.0	0.214 " "

Fig. 9 shows $\Delta C_{l_{max}}$ versus percent camber for theoretical and experimental values, where the experimental

value was obtained from Fig. 4, by subtracting $C_{l_{max}}$ of the symmetrical model from the $C_{l_{max}}$ of the three other configurations, and the theoretical value was taken to be equal to C_{l_b}, as given by thin airfoil theory. Here it is seen that the values for the three percent and six percent cambered models, suffering from boundary layer thickening or separation at the trailing edge, fall short of the theoretical value, but on the other hand, the value for the slotted six percent cambered model and the theoretical value are coincident. It is noted that for the three percent cambered model, the actual value is about 92 percent of the theoretical value.

Fig. 10 shows the lift curves of the symmetrical model and the slotted six percent cambered model, and the translated symmetrical curve, which has been shifted upwards by an amount equal to the theoretical value of C_{l_b} (0.748), and shifted to the right by an amount equal to the experimental value of ideal angle of attack, $\alpha_{i_{ex}}$ (4.5°). It is seen that the agreement is good.

Thus it is seen that the linearized theory will give good results in the prediction of $\Delta C_{l_{max}}$, provided trailing edge separation can be controlled, but that the theory fails to provide a reasonable prediction for ideal angle of attack, due to viscous effects, in which boundary layer thickening causes the stagnation point to move forward on the under surface of the airfoil.

Since good agreement between theoretical and experimental

values for portions of the hypothesis was obtained, it is felt that further investigation of this idea is warranted, using greater Reynolds Numbers and investigating the effects of thickness variations as well as more camber variations.

SUMMARY OF MAIN RESULTS

1. The addition of camber to a nose-stalling airfoil tends to make it a trailing edge staller or partially so, but some form of boundary layer control can shift the stall back to the nose.

2. Table II summarizes the important airfoil characteristics. In Table II the theoretical value of C_{l_o} is given by

$$C_{l_o} = C_{l_b} - a\alpha_i$$

where C_{l_b} and α_i were computed using the previously given thin airfoil formulae.

The experimental value of C_{l_o} and C_{l_b} was taken from the data in Fig. 4, the value of C_{l_b} being taken at the experimental value of α_i.

3. The lift curve slope varies from 4.9 to 5.5, which is considerably less than the theoretical value of 2π. This is a viscous effect; the boundary layer thickens toward the trailing edge and thus causes loss of circulation. Also leakage around the end plate may be causing some reduction in the slope.

4. The measured values of C_{l_o} for the cambered airfoils are less than the theoretical values from thin airfoil theory, due to loss of circulation caused by boundary layer thickening at the trailing edge.

5. The experimental ideal angle of attack is larger than the theoretical value, which is also due to the viscous effects, since loss of circulation corresponds to a shift of the stagnation point farther forward on the lower surface of the airfoil.

6. $\Delta C_{l_{max}}$ for the unslotted airfoil is less than the theoretical value, C_{l_b}, since loss of circulation at the trailing edge is not controlled. However, for the three percent cambered model, this discrepancy is less than ten percent.

7. For the slotted airfoil, there is a basic loss of circulation, which is even greater than for the unslotted airfoil; C_{l_o} is less and α_i is greater. This additional loss, at low angles of attack, is connected with the slot. However, at high angles of attack, the slot prevents any further loss of circulation, so that the stall is controlled by the nose in the same manner as for the symmetrical airfoil. This is shown by the similarity of the nose pressure distribution at corresponding α_i; and it results in fairly good agreement with the theoretical prediction $\Delta C_{l_{max}} = C_{l_b}$.

REFERENCES

1. McCullough, G. B. and Gault, D. E.: "Examples of Three Representative Types of Airfoil - Section Stall At Low Speed." NACA TN 2502, 1951.

2. Roshko, A.: "Pressure Distribution At The Nose Of A Thin Lifting Airfoil." Douglas Aircraft Report No. SM-23368, 1958.

3. Roshko, A.: "Unpublished Note."

4. Spence, D. A. and Beasley, J. A.: "The Calculation Of Lift Slopes, Allowing For Boundary Layer, With Applications To The R. A. E. 101 and 104 Aerofoils." Royal Aircraft Establishment Report AERO. 2598, 1958.

TABLE I

AIRFOIL COORDINATES AND MEAN LINE DATA

Symmetrical		3 Mean Line		6 Mean Line		3 Camber				6 Camber			
x	y	y_c	dy_c/dx	y_c	dy_c/dx	x_u	y_u	x_l	y_l	x_u	y_u	x_l	y_l
0.00	0.00	0.00	.131	0.00	.262								
.50	.70	.07		.13									
.75	.86	.10		.20									
1.25	1.11	.16		.33									
2.50	1.56	.33		.66									
5.00	2.17	.66		1.31									
7.50	2.61	.98	.131	1.97	.262								
10.00	2.96	1.31	.112	2.62	.225	9.67	4.28	10.33	-1.65	9.35	5.51	10.65	-0.26
15.00	3.50	1.83	.094	3.66	.188	14.67	5.31	15.33	-1.65	14.36	7.09	15.64	+0.22
20.00	3.88	2.25	.075	4.50	.150	19.72	6.12	20.28	-1.62	19.42	8.34	20.58	0.66

TABLE I (Cont'd)

AIRFOIL COORDINATES AND MEAN LINE DATA

Symmetrical		3 Mean Line		6 Mean Line		3 Camber				6 Camber			
X	Y	Y_c	dY_c/dX	Y_c	dY_c/dX	X_u	Y_u	X_L	Y_L	X_u	Y_u	X_L	Y_L
25.00	4.16	2.58	.056	5.16	.112	24.77	6.73	25.23	-1.57	24.54	9.29	25.46	1.02
30.00	4.35	2.81	.038	5.62	.075	29.84	7.16	30.16	-1.53	29.68	9.96	30.32	1.29
40.00	4.50	3.00	0.000	6.00	0.000	40.00	7.50	40.00	-1.50	40.00	10.50	40.00	1.50
50.00	4.34	3.92	-.017	5.83	-.033	50.07	7.25	49.93	-1.42	50.14	10.17	49.86	1.50
60.00	3.74	2.67	-.033	5.33	-.067	60.12	6.41	59.88	-1.08	60.25	9.07	59.75	1.60
70.00	2.86	2.25	-.050	4.50	-.100	70.14	5.10	69.86	-0.60	70.28	7.34	69.72	1.66
80.00	1.80	1.67	-.067	3.33	-.133	80.12	3.47	79.88	-0.14	80.23	5.12	79.77	1.54
90.00	.74	0.92	-.083	1.83	-.167	90.06	1.65	89.94	+0.18	90.12	2.56	89.88	1.10
95.00	.28	0.48	-.092	.96	-.183	95.02	.76	94.98	0.20	95.05	1.23	94.95	.68
100.00	0.00	0.00	-.100	0.00	-.200	100.00	0.00	100.00	0.00	100.00	0.00	100.00	0.00

TABLE II

SUMMARY OF AIRFOIL CHARACTERISTICS

q = 20 psf	Theoretical				Experimental				
Model	a	α_i	C_{l_o}	C_{l_b}	a	α_i	C_{l_o}	C_{l_b}	$\Delta C_{l_{max}}$
Symmetrical	2π	0.000	0.000	0.000	4.9	0.5	-.21	-.206	0.000
3 % Camber	↑	.321	.339	.374	5.1	1.5	.245	.379	.344
6 % Camber		.642	.678	.748	5.1	3.25	.528	.818	.600
6 % Camber (Slot Taped)	↓	.642	.678	.748	5.1	--	.461	--	.599
6 % Camber (Slotted)	2π	.642	.678	.748	5.1	4.5	.362	.762	.750
q = 40 psf									
Symmetrical	2π	0.000	0.000	0.000	5.3	0.5	-.21	-.205	0.000
3% Camber	↑	.321	.339	.374	5.5	1.5	-.243	.387	.347
6 % Camber		.642	.678	.748	5.5	3.25	.507	.817	.589
6 % Camber (Slotted)	2π	.642	.678	.748	5.5	4.5	.348	.780	.745

a = the slope of the lift curve

α_i = ideal angle of attack

C_{l_o} = lift coefficient at zero angle of attack

C_{l_b} = lift coefficient at ideal angle of attack

$\Delta C_{l_{max}}$ = maximum lift coefficient minus the maximum lift coefficient of the symmetrical model

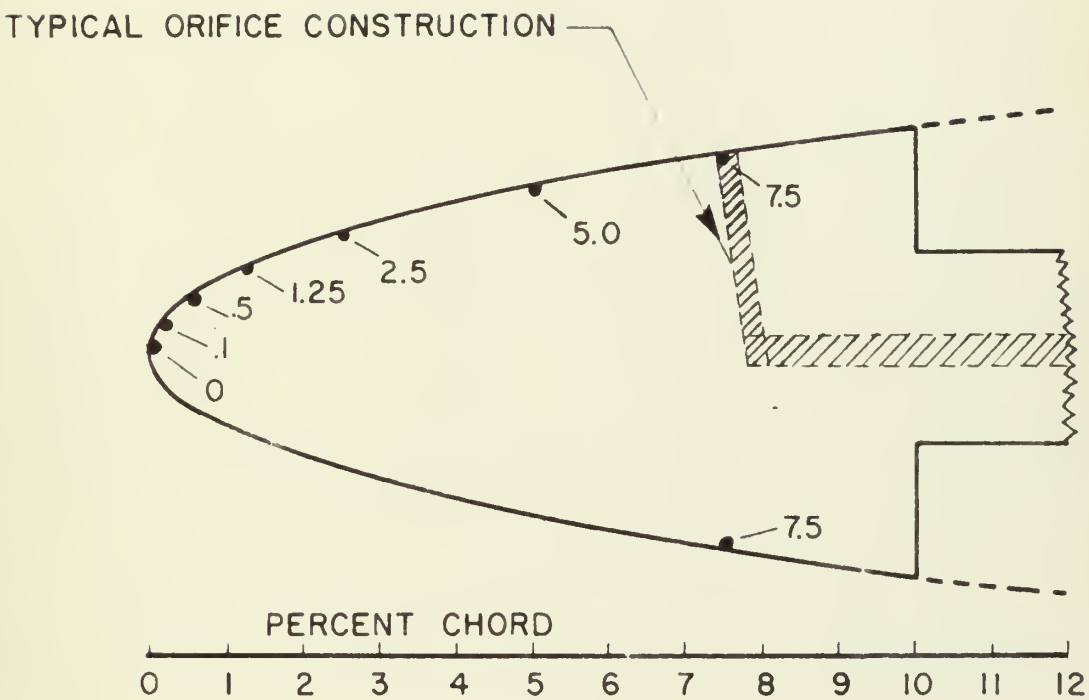

FIG. 1 BRASS NOSE SHOWING ORIFICE LOCATIONS

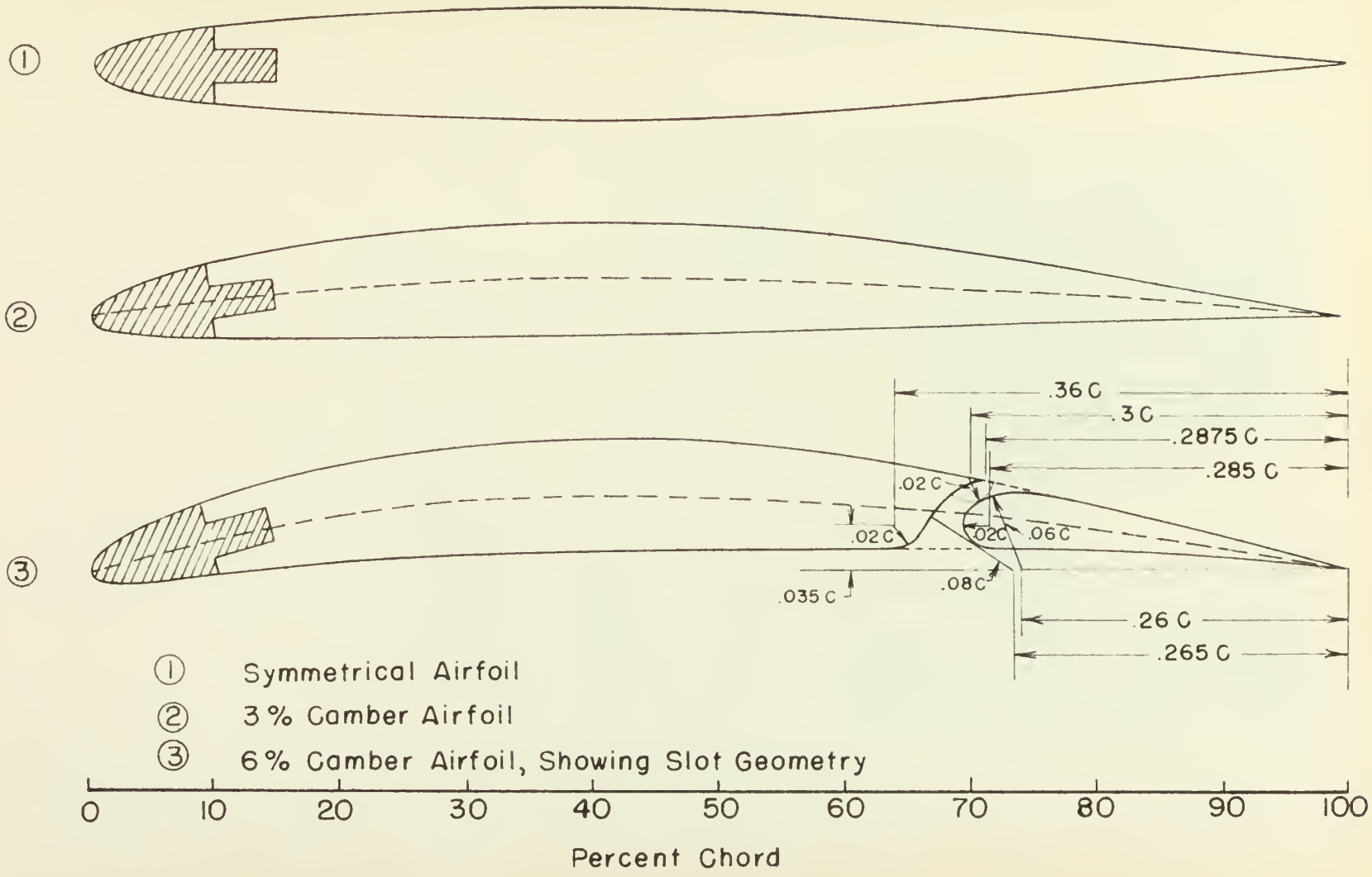

FIG. 2 – AIRFOIL SECTIONS

Fig. 3. Slotted Six Percent Cambered Model in Tunnel Test Section. (One End Plate Removed)

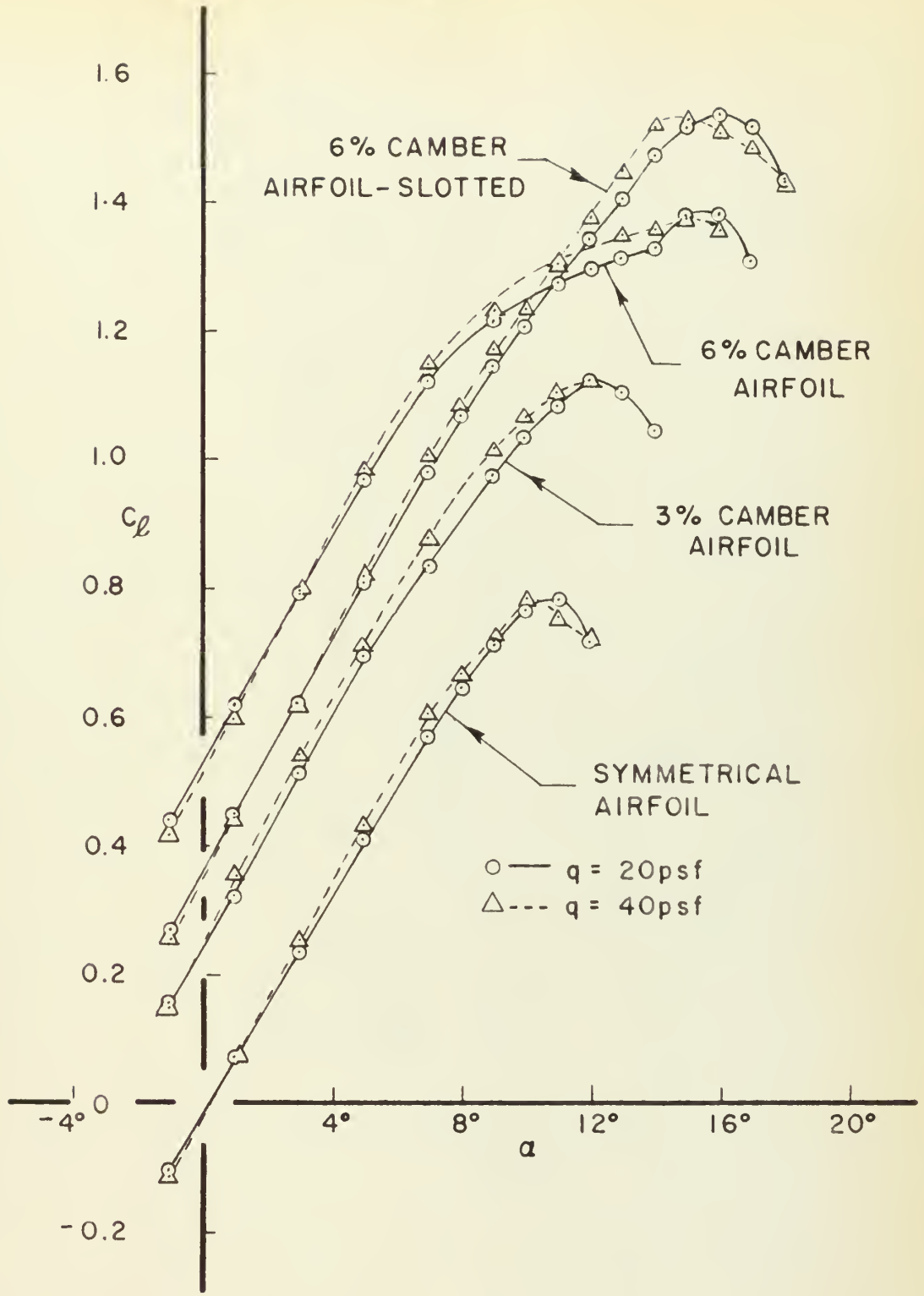

FIG. 4 LIFT COEFFICIENT VS. ANGLE OF ATTACK

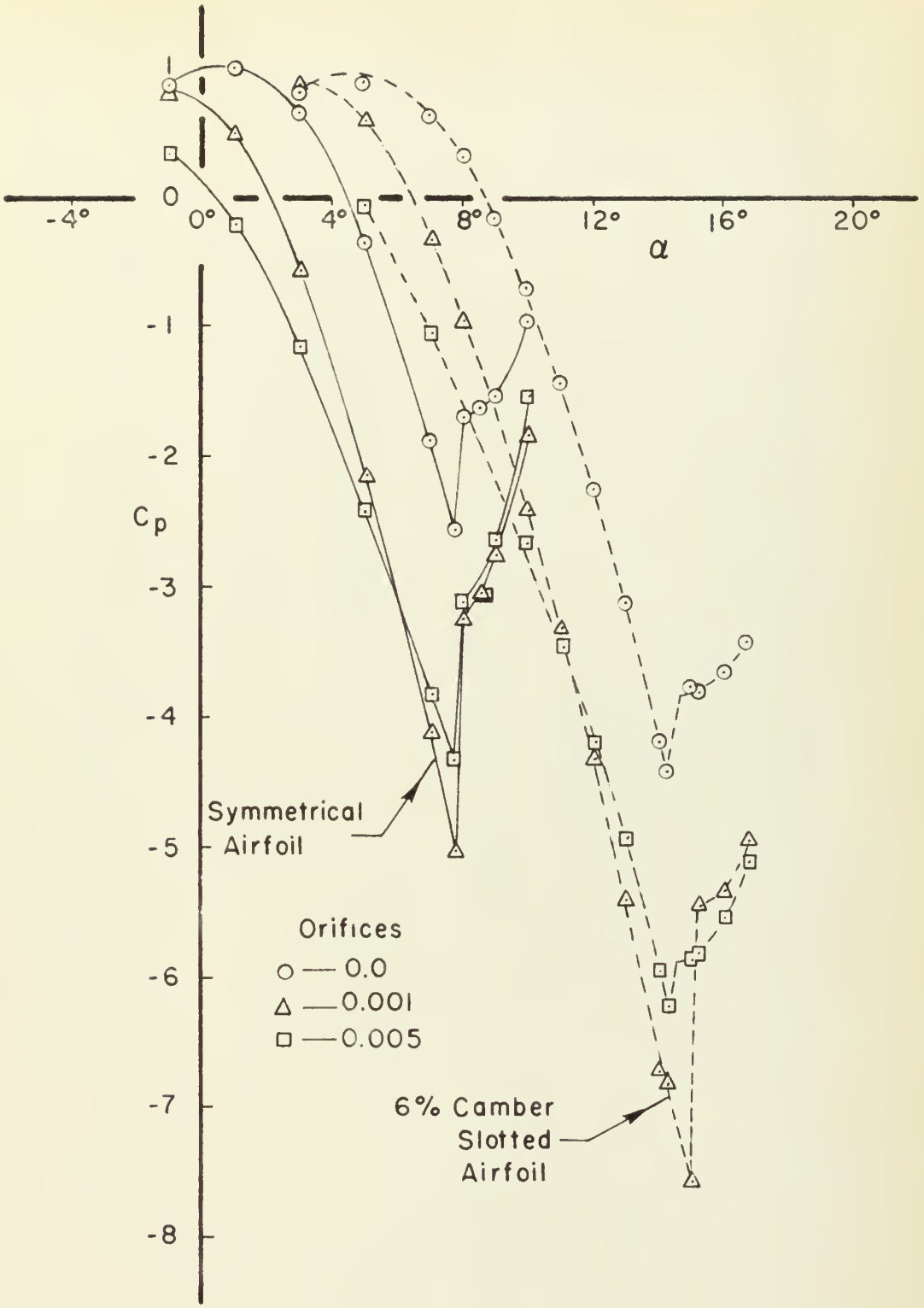

FIG. 5 PRESSURE DISTRIBUTION ON THE NOSE VS. ANGLE OF ATTACK (q = 40 psf)

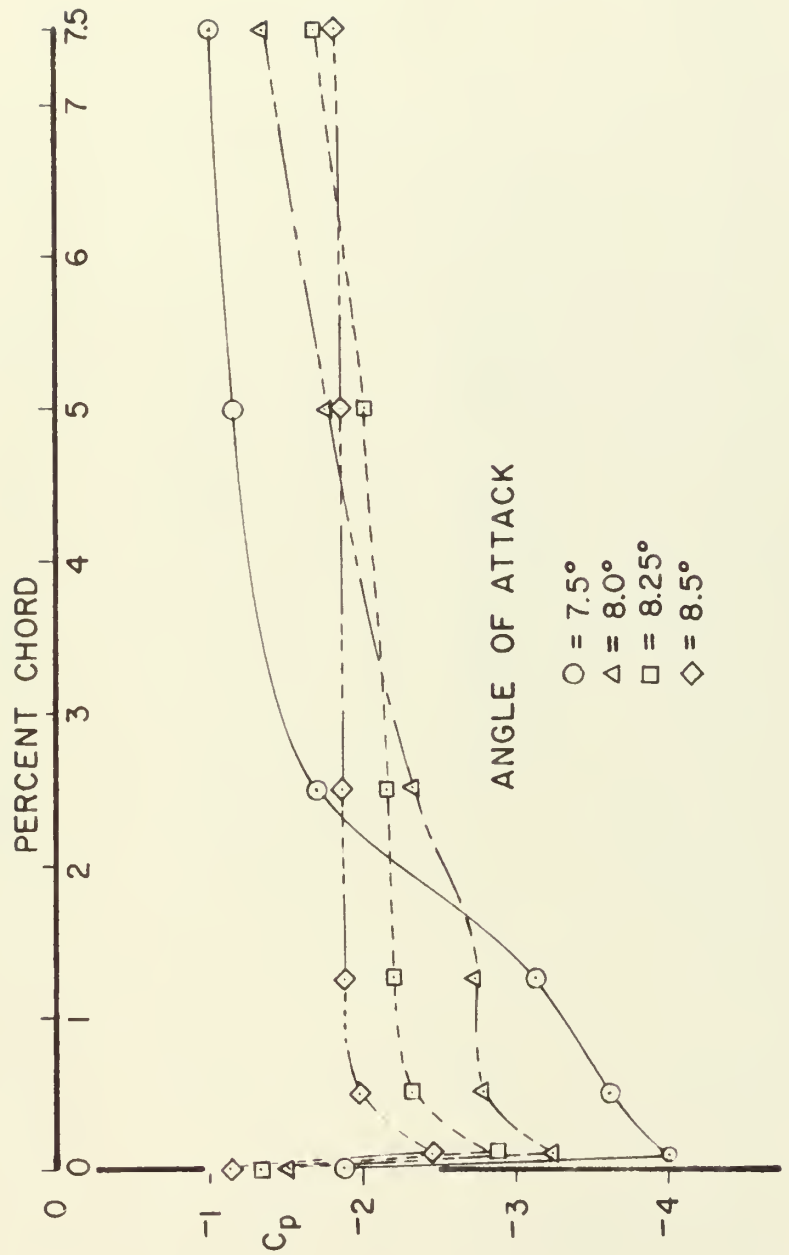

FIG. 6 CHORDWISE PRESSURE DISTRIBUTIONS ON SYMMETRICAL AIRFOIL
(q = 20 psf)

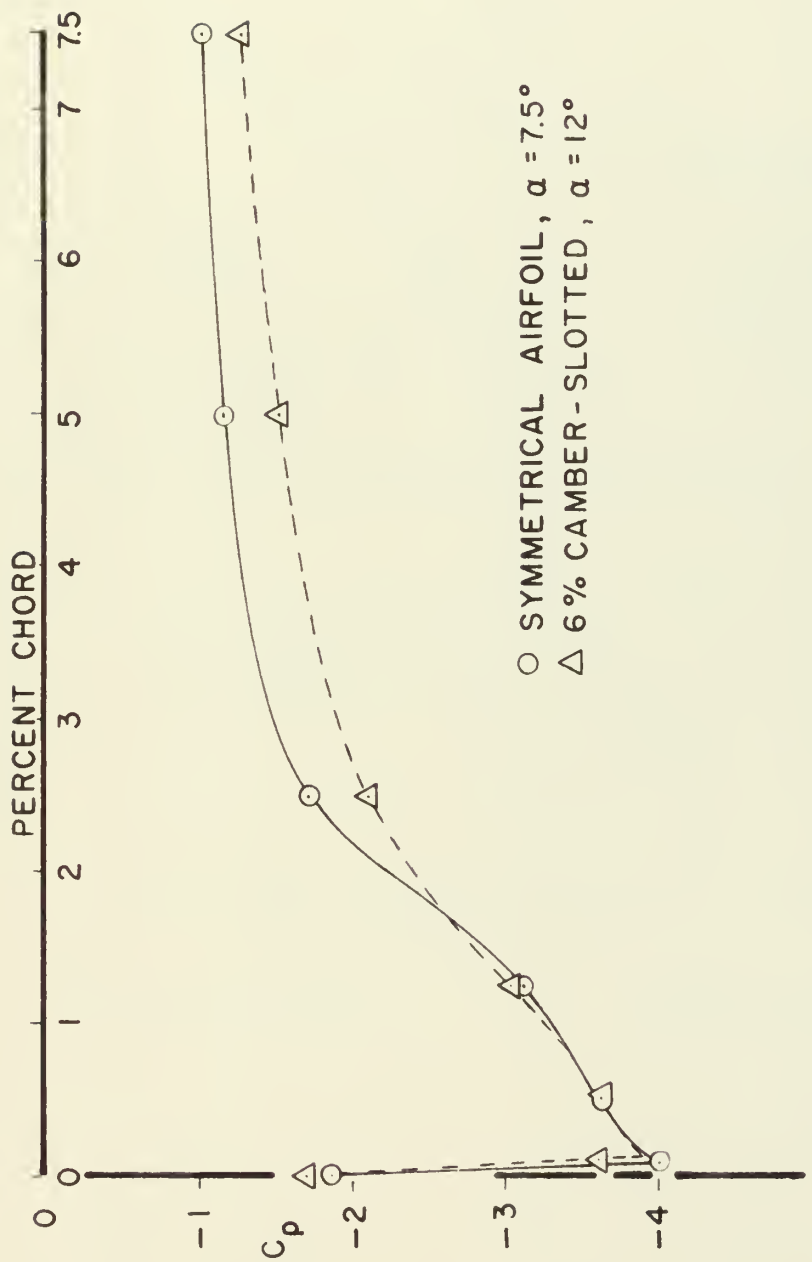

FIG. 7 PRESSURE DISTRIBUTIONS AT A GIVEN VALUE OF $(\alpha - \alpha_i)$
($q = 20$ psf)

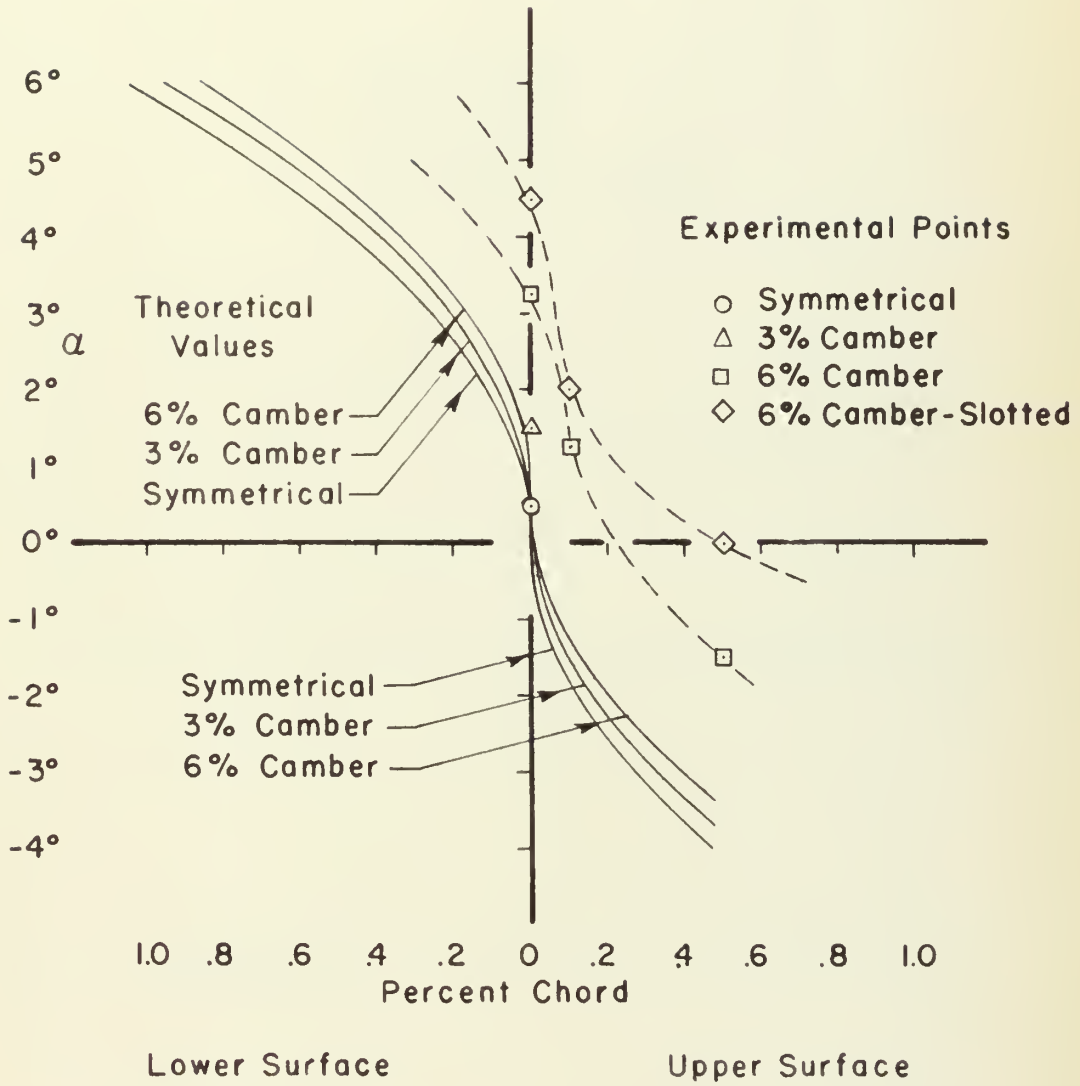

FIG. 8 LOCATION OF STAGNATION POINT VS. ANGLE OF ATTACK

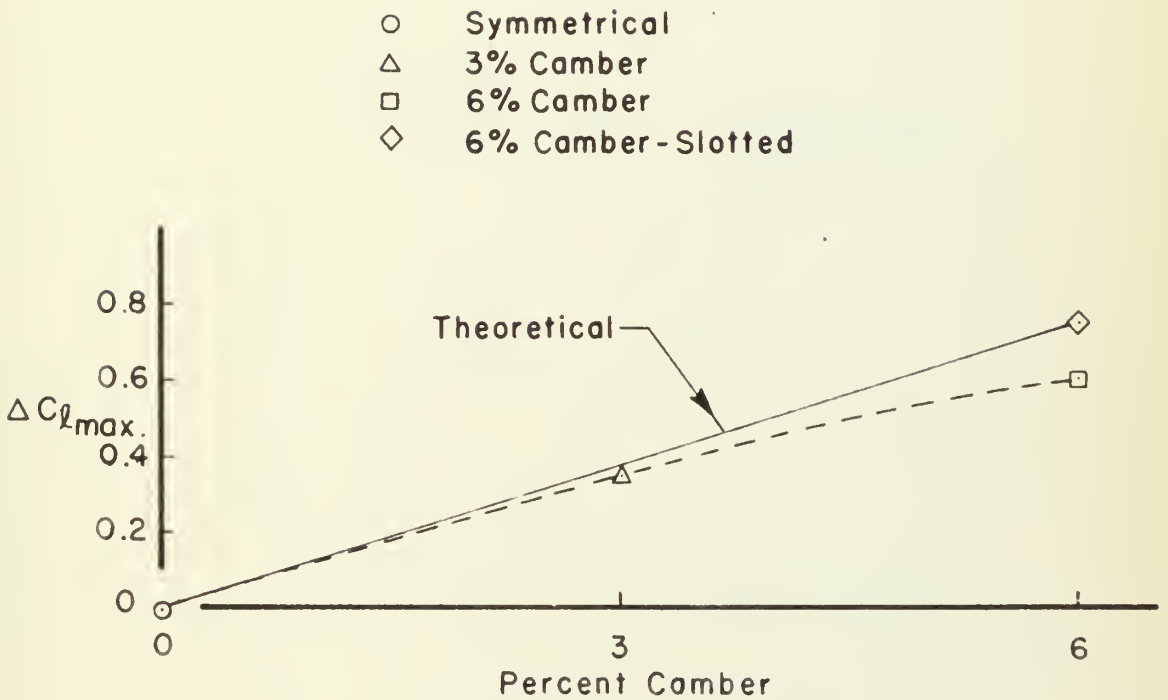

FIG. 9 DIFFERENCE IN MAXIMUM LIFT COEFFICIENT VS. CAMBER

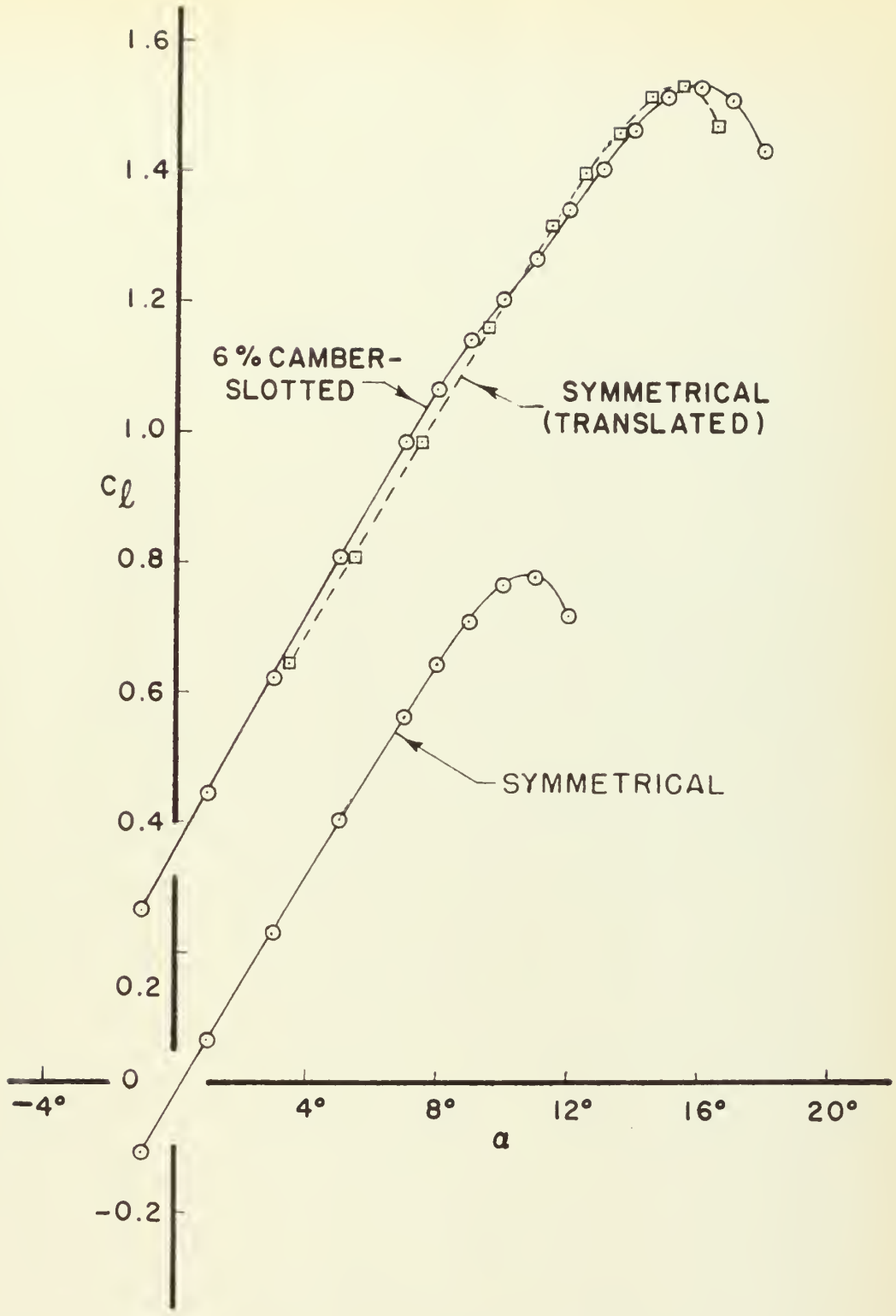

FIG. 10 PREDICTION FOR CAMBERED AIRFOIL FROM RESULTS ON SYMMETRICAL AIRFOIL
(q=20psf)